

Image blur investigation using EUV-Interference Lithography

T. Allenet^a, J. G. Santaclara^b, G. Rispens^b, B. Geh^{c,d}, Y. Ekinci^a

^a Paul Scherrer Institut, 5232 Villigen-PSI, Switzerland

^b ASML, De Run 6501, 5504 DR Veldhoven, The Netherlands

^c Carl Zeiss SMT, Rudolf-Eber-Straße 2, 73447 Oberkochen, Germany

^d ASML TDC, 399 W. Trimble Road, San Jose, CA 95131, USA

email: timothee.allenet@psi.ch

ABSTRACT

As EUV lithography moves into mass production, photoresist development continues to be one of the most prominent challenges to reach higher resolutions. This work aims to address the resist performance limitations with regards to image blur. Feature quality is a result of the aerial image and the response function of the resist. The contrast of the aerial image is reduced by the exposure tool (optical aberrations and mechanical stability) and the resist (chemical mechanisms and development). Decoupling these two contributions would be highly valuable information to assist in resist development. Here, we investigate the through-pitch behavior of image contrast to determine and de-correlate the limitations of the resist and the exposure process. The method used here is based on the experimental analysis of the through-pitch behaviors of CD and LWR in dense lines/space patterns using EUV interference lithography.

Keywords: EUV, interference lithography, contrast loss, k_4 metric, resist blur

1. Introduction

As EUV lithography has moved into HVM, high-NA EUVL is the most promising technology to continue assisting the industry with future technology nodes¹. Resist development has been identified as one of the significant challenges to deliver yet higher resolutions required for future technology nodes. Within resist performance assessment, a conventional way to study materials is to consider the well-known RLS trade-off² (resolution, linewidth roughness, and sensitivity). Pitch-dependent metrics such as the Z-factor³ have been used to quantify and to compare the resist performance over the years. This approach is straightforward and easily handled but constitutes a crude assessment metric since it does not give insights about the underlying contributions. More recently, analytical developments have been put forward to push our understanding of latent image formation with regards to the complex lithographic information transfer. New metrics have been introduced in an attempt to disentangle and understand the different contributions of the exposure process. Although analytical developments have allowed estimating different contributions⁴, image blur as a convolution of tool and resist factors ultimately limits the physical understanding of each contribution. Developing a specific measurement method for the image blur is therefore of interest for further investigation of resists.

In this work, we consider a method to experimentally measure the image blur. In order to do so, the EUV-IL (Interference Lithography) tool at Paul Scherrer Institute (PSI) is used as an alternative to EUV scanners for resist screening⁵. In IL, the aerial image of lines/spaces is generated by the interference pattern of two plane waves, which provides a well-defined contrast⁶. In theory, two-beam interference provides a sinusoidal aerial image with a constant contrast independent of the pitch. We designed and fabricated masks with transmission diffraction gratings and carried out EUV-IL exposures at 13.5 nm wavelength to pattern lines/spaces. To characterize the through-pitch resist performance the patterns are imaged by SEM and analyzed with an in-house software.

We developed a simplistic model in which the ideal contrast of sinusoidal aerial image of the EUV-IL and the measurement of resist performance through the pitch allows extraction of the resist blur. Characterization of resist parameters using LWR data is used to verify proof of concept by comparing k_4 metric values to scanner results⁴. The method is then extended to EL (Exposure Latitude) study to isolate image blur as a single free-space parameter.

2. Method

In interference lithography, the interference pattern between two or more coherent beams results in a periodic aerial image, which is used to expose and pattern photoresists. Figure 1 shows the EUV-IL exposure tool with transmission optics used at the Swiss Light Source at PSI. A synchrotron light source is used to generate a coherent beam with $\lambda=13.5$ nm, which is spatially filtered through mirrors and pinholes. Masks with adjacent transmission gratings are illuminated to generate diffracted beams designed to interfere at the wafer level, resulting in an aerial image for resist patterning. With this physical principle, periodic features can be obtained: two-beam masks are used to obtain lines/spaces patterns, whereas 4-beam masks can be used to obtain contact-hole patterns.

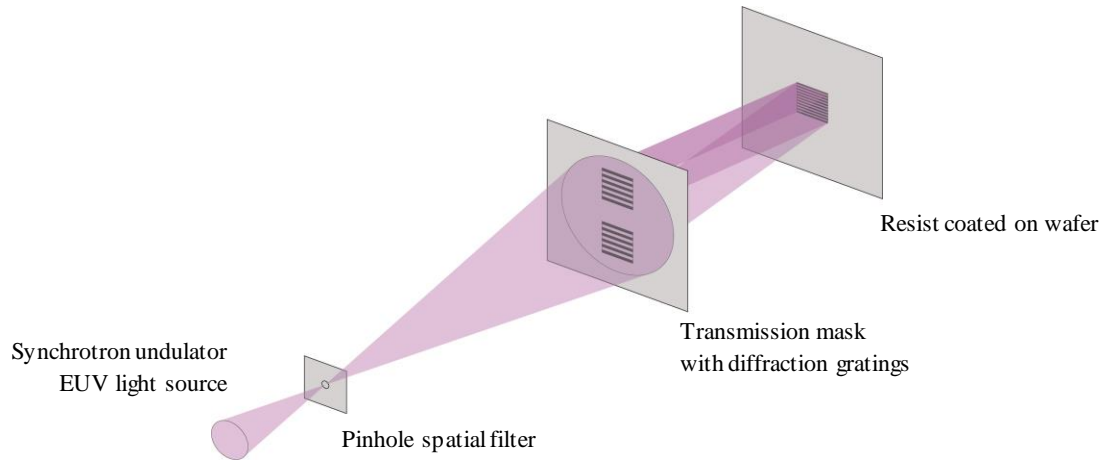


Figure 1: Schematic representation of EUV interference lithography exposure tool where a coherent $\lambda = 13.5$ nm beam and transmission masks consisting grating pairs. First-order diffraction is used for interfering beams. The wafer coated with the photoresist is placed where the maximum overlap of the interfering beams occurs. In this schematics, only two gratings and first-order diffraction beam are shown for clarity.

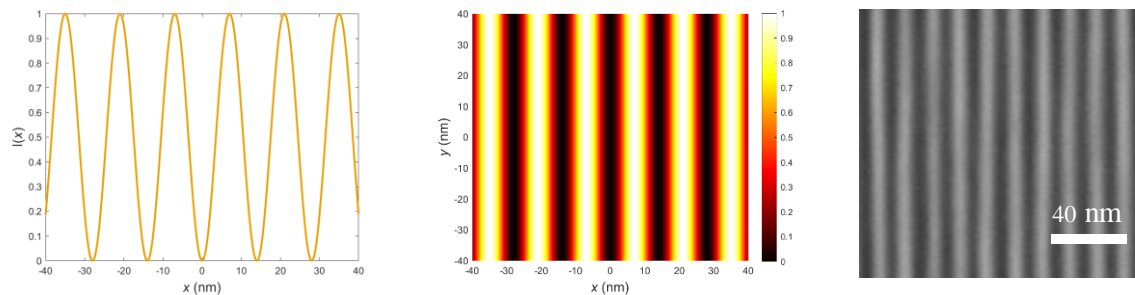


Figure 2: Theoretical ideal sinusoidal aerial image with a contrast of 1 obtained with IL. Left: Normalized cross-section of the aerial image. Middle: Top view of the aerial image. Right: HSQ patterns with 7 nm HP obtained with EUV-IL⁷.

Characterization of resist performance through lines/spaces patterns is sought out in the interest of image blur measurement. Therefore interference between two-beam diffraction gratings is used to provide an ideal sinusoidal aerial image, as is shown in **Error! Reference source not found.** 1st order two-beam masks allow for a linewidth theoretical resolution limit of 7 nm, which was achieved and also shown in Figure 2.

The use of an IL exposure tool is of particular interest in the measurement of image blur. The simple optical setup and the interference lithography concept allow for a well-defined aerial image⁸. Most importantly, the exploited interference principle produces a sinusoidal aerial image with a constant theoretical contrast of 1.

Image blur is a convolution of two blur components: the aerial image quality obtained with a tool (image contrast, shot noise, optical aberrations, mechanical stability, focus blur, etc.) and resist response (material stochasticity, photoacid generation, diffusion, development, etc.). To investigate the impact of image blur, we consider a one-dimensional image modulation along the x -axis. The interference lithography produces a simplified sinusoidal aerial image^{8,9}. For an intensity distribution with amplitude modulation A , a period p and a wave-vector $k = 2\pi/p$, the aerial image intensity is given as

$$I(x) = \frac{A}{2} (1 - \cos(kx))$$

By assuming a Gaussian blur model of the image blur as

$$G(x) = \frac{1}{\sqrt{2\pi}\sigma} \cdot e^{-\frac{x^2}{2\sigma^2}} \quad (1)$$

where σ is the image blur quantity, we can estimate the subsequent aerial image signal by considering the following convolution⁴:

$$I_{\text{blurred}} = I(x) \otimes G(x) = \frac{A}{2} \left(1 - e^{-2\left(\frac{\pi\sigma}{p}\right)^2} \cdot \cos(kx) \right) \quad (2)$$

Given the assumptions made, theoretical estimations of an ideal and a blurred aerial image are shown in Figure 3. This elementary representation allows us to observe the loss of signal contrast between the ideal and the blurred signal, in which the contrast is defined as

$$C = (I_{\text{max}} - I_{\text{min}}) / (I_{\text{max}} + I_{\text{min}}). \quad (3)$$

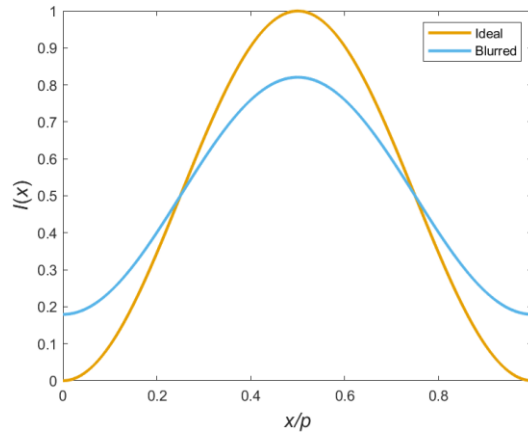


Figure 3: Representation of an ideal ($C=1$) and Gaussian blurred ($C=0.64$) sinusoidal aerial image obtained with EUV-IL showing a contrast loss due to the image blur.

For a pitch-independent image blur and the constant contrast of the aerial image, the impact of the blur becomes more significant with decreasing pitch, as it can be observed in Figure 4. This principle of pitch-dependent contrast loss for a constant image blur and well-defined aerial image can be used to measure image blur.

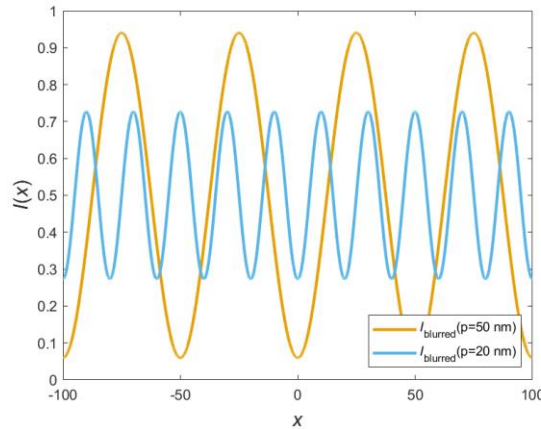


Figure 4: Demonstration of the pitch-dependent contrast loss of a sinusoidal aerial image due to the image blur. The effective aerial images (blurred images) are plotted for pitches of 50 nm and 20 nm for a blur quantity of 4 nm.

The quality of an aerial image can be characterized by its Normalized Image Log-Slope,

$$NILS = L \frac{\partial \ln I(x)}{\partial x} \quad (4)$$

where L is the linewidth of the patterned feature. In an ideal aerial image ($C=1$), $NILS$ reaches π for a nominal linewidth L equal to half-pitch at the ideal threshold. In reality, the blurred aerial image exhibits a contrast loss from its ideal representation, which leads to $NILS = \mu\pi$ with $\mu \in [0,1]$. Therefore we can extend our Gaussian blur model to describe the variation of the blurred image $NILS$ through pitch:

$$NILS_{blurred} = NILS \cdot e^{-2\left(\frac{\pi\sigma}{p}\right)^2} \quad (5)$$

For the characterization of image blur, experimental metrics are necessary. A recent investigation of LWR behavior through pitch⁴ can be applied here, leading to:

$$LWR = k_4 \cdot \sqrt{\frac{h\nu}{D}} \cdot e^{\frac{1}{2}\left(\frac{\pi\sigma}{p}\right)^2} \cdot \frac{p}{\pi} \quad (6)$$

with the resist parameter k_4 , source energy $h\nu$ (eV), resist dose-to-clear D (mJ/cm²) as well as image blur σ . This method was introduced to extract the k_4 factor as a pure resist metric governed by absorption and quantum efficiency⁴. In this case, image blur is fitted to obtain a constant k_4 through pitch, which provides an indirect way of measuring σ . An alternative way to extract image blur directly is of interest. For this, we consider the study of EL through-pitch.

In an ideal image, $EL = 10 \cdot NILS$ with $NILS = \pi$. By considering the $NILS_{blurred}$ expression depicted above, we can estimate image contrast loss as a function of image blur by normalizing EL through pitch:

$$\frac{EL}{10 \cdot NILS} = e^{-2\left(\frac{\pi\sigma}{p}\right)^2} \quad (7)$$

This approach can be used to extract the image blur σ as a single free-space parameter through pitch, considering an ideal sinusoidal aerial image obtained with EUV-IL with a contrast of 1 and a $NILS$ of π .

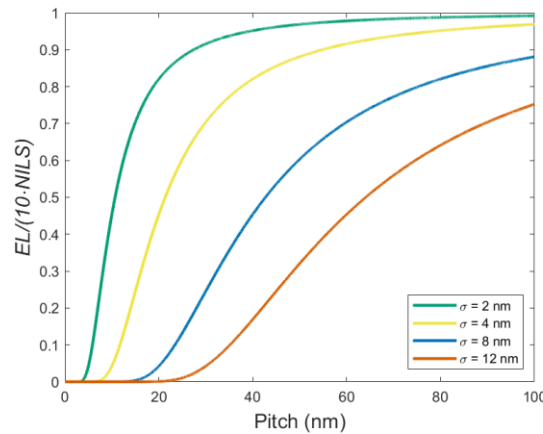


Figure 5: Estimation of aerial image degradation through pitch considering a gaussian blur for an ideal sinusoidal wave with a contrast of 1 and $NILS$ of π .

Figure 5 shows image degradation through pitch for different blur values. We observe rapid decay of image quality with a slightly increasing blur. Most importantly, we can observe that in the case of an ideal tool, an image blur of 3 nm is necessary in order to reach sub-10nm features with a contrast higher than 0.5. This can be used as a general qualitative guideline for tool development: image blur of 3 nm and lower is absolutely necessary for the deployment of high-NA tools.

Investigation of lines/spaces LWR and EL through pitch is, therefore, used to observe image quality degradation for high resolution and ultimately quantify image blur experimental limits. In the following section, we describe the experimental procedures used for this study.

3. Experimental methods

Two-beam transmission grating masks are used to pattern lines/spaces on coated resists. As shown in Figure 6, the gratings have been designed to obtain interfering fields on the wafer for image modulation and resist patterning. m^{th} order diffraction fields allow for a frequency multiplying of the mask gratings (period g) on subsequent wafer gratings (period p):

$$p = \frac{\lambda}{\sin \theta} = \frac{g}{2m} \quad (8)$$

Thin free-standing Si_3N_4 membranes on silicon frames are elaborated for mask support. Transmission gratings are obtained after spin-coating and patterning hydrogen silsesquioxane (HSQ) via electron beam lithography. Mask layout is designed with different pairs of gratings to obtain different pitches at the wafer level with a single mask. A thick Nickel layer is electroplated around the gratings as a photon stop to isolate the transmission grating signal. Figure 7 shows SEM images of a mask designed specifically for wide pitches ranging from 100 to 40 nm on the wafer, as well as an image of an HSQ mask grating.

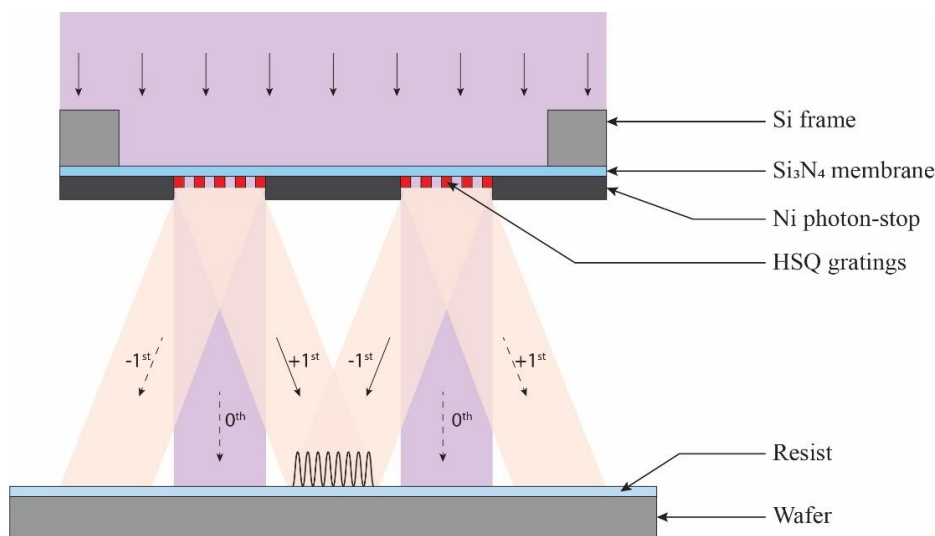


Figure 6: Schematic representation of EUV-IL at the wafer level with 1st order transmission mask. Transmission gratings on the mask are used to pattern coated resists with 1st order interfering diffraction beams. Subsequent flood exposures of 0th and outward 1st order fields are represented with dashed arrows. For simplicity, only the 0th and 1st order diffraction beams are shown.

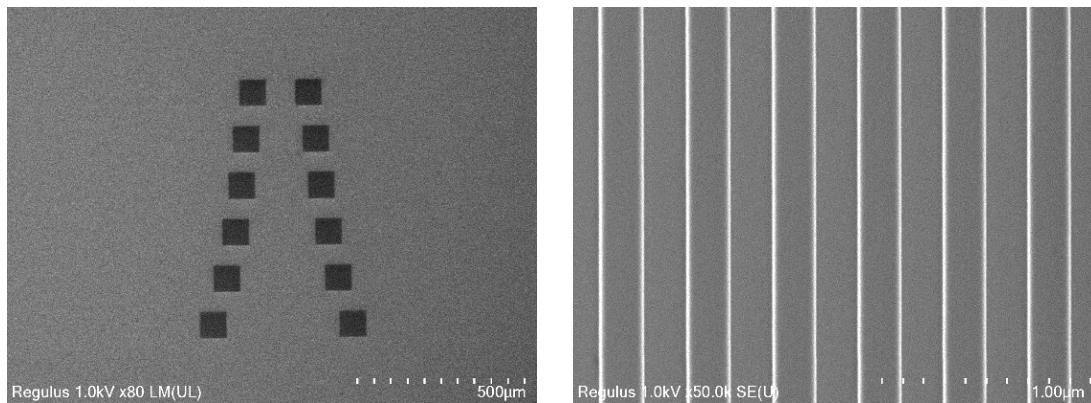


Figure 7: SEM images of a mask. Left: SEM image showing the layout of the different pairs of transmission gratings. It should be noted that the grating pairs are designed with an increasing inter-grating distance to provide the aerial image at the same wafer distance. Left: SEM image of a grating obtained with e-beam lithography patterned HSQ.

Another useful feature of the EUV-IL is the fact that the aerial image has infinite depth of focus, i.e. the contrast is independent of focus. Therefore the exposure simply consists of a dose-step matrix and does not need a through-focus matrix. Figure 8 shows an overexposed field of a single dose-step exposure, which shows the interference pattern field in the center and 0th and negative 1st order flood exposures to their sides.

Imaging of resist patterns is carried out by scanning electron microscopy (Hitachi Regulus 8230). An open-source pattern analysis software (SMILE¹⁰) is used to detect line edges of input images, as shown in Figure 9.

The software is used to measure CD and unbiased LWR. Acquired CD and LWR_{unb} data are plotted through dose and fitted in order to measure pitch-specific Dose-to-Size (DtS), corresponding LWR_{unb} and EL, defined as the dose range for $\pm 10\%$ change in CD around target CD (TCD):

$$EL(\%) = \frac{D(TCD + 10\%) - D(TCD - 10\%)}{DtS} \cdot 100 \quad (9)$$

An example of a raw data set is shown in Figure 10.

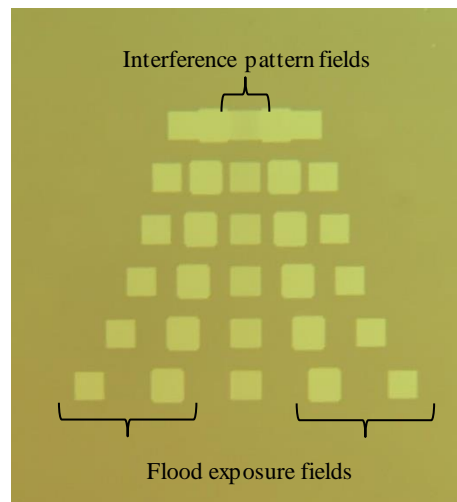


Figure 8: Optical microscope image of a wafer with a single EUV-IL dose-step exposure showing the 1st order interference fields for the pitches ranging from 200 to 40 nm as well as the 0th and the negative first-order flood exposures.

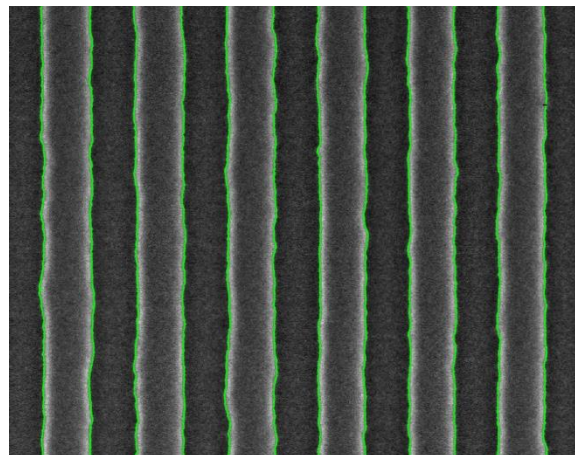


Figure 9: SEM image of a lines/space pattern after running through a line detection software.

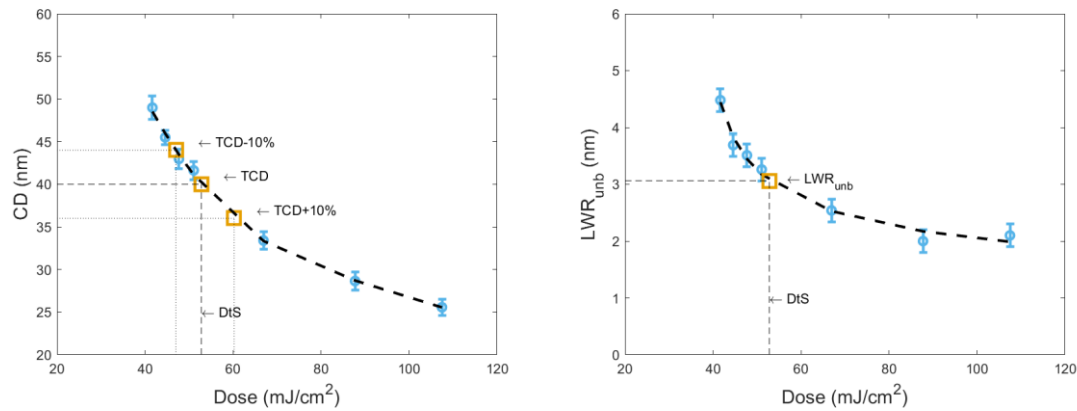


Figure 10: Raw CD and LWR_{unb} as a function of dose used for fitting and extraction of pitch specific DtS, EL, and LWR_{unb} parameters.

4. Results

To validate the experimental approach considered here, we started by selecting a state-of-the-art chemically amplified resist (CAR) to compare with previously published results. Through-pitch exposures ranging from 100 nm half-pitch (HP) down to the observed resist resolution limit of 13 nm HP were carried out with different masks. Figure 11: Measured LWR_{unb} results through HP for a state-of-the-art CAR. Data fitting with the k_4 metric equation is used to extract k_4 and image blur values. shows the subsequent results of LWR_{unb} as a function of HP.

We consider the k_4 metric equation with a source $h\nu = 92$ eV, ideal $NILS = \pi$, and resist dose to clear, which was measured at 27 mJ/cm². Fitting of the measured data allowed us to extract an image blur value of 5.5 ± 0.6 nm and a k_4 factor of 0.10 ± 0.01 . These results are in close agreement with previously published values obtained with an NXE:3400 0.33NA scanner⁴. This convergence of results between different exposure tools allows us to verify the theoretical assumptions made in the first section of this paper about the aerial image and the Gaussian blur model.

Having obtained converging results of resist characterization through LWR study between alternative EUV exposure tools, the extension of the blur measurement via EL investigation is attempted. A low-resolution resist was preferred for a first-hand assessment of the feasibility of blur measurement through EL in order to avoid the tool resolution limit regime. A well-known inorganic resist was selected and characterized through pitch from 100 nm half-pitch down to an observed resist resolution limit of 25 nm. Figure 12 shows the results of normalized EL through pitch by considering an ideal $NILS = \pi$.

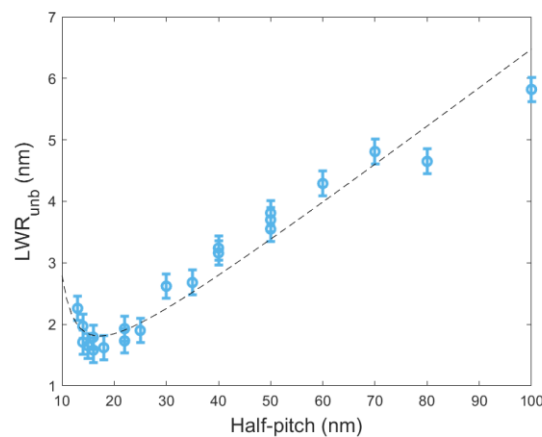


Figure 11: Measured LWR_{unb} results through HP for a state-of-the-art CAR. Data fitting with the k_4 metric equation is used to extract k_4 and image blur values.

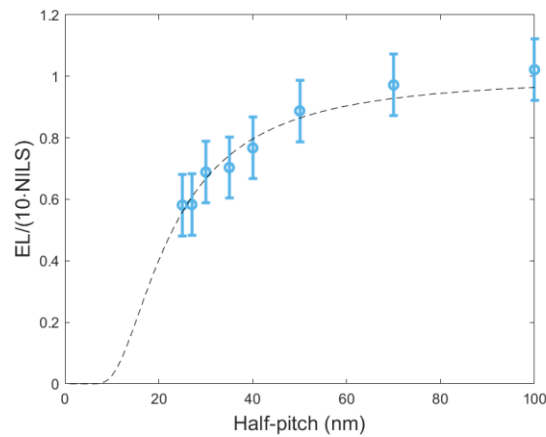


Figure 12: Normalized EL results through half-pitch for an ideal $NILS = \pi$ measured with an 2inorganic resist.

Results show an exponential decay of normalized EL values when approaching the lower half-pitch, in agreement with our theoretical assumptions. Data fitting allowed for an extraction of image blur $\sigma = 8.6 \pm 0.6$ nm, which is significantly higher than the high-resolution CAR tested previously. Direct extraction of image blur as a single free-standing parameter of EL as a function of pitch is therefore verified.

5. Conclusions and Outlook

This work aims to study image blur, defined as a convolution between the aerial image and resist induced blur. Theoretical assumptions were made to provide a model for image blur behavior and impact. This has helped to identify a performance milestone of a 3-nm image blur to reach high-NA exposure tool applications. A method was put forward to experimentally determine image blur through analysis of lines/spaces patterns exposed with the EUV-IL tool at PSI. For that, the pitch dependency of LWR_{unb} and EL was considered in order to extract resist parameters with experimental results. Preliminary results with a high-resolution CAR as well as a low-resolution inorganic resist results allowed to validate the method, thereby opening up the approach for a more systematic investigation and elaborate studies.

In future work, we would like to extend this study to higher resolutions and different resist platforms. This approach should allow for the disentanglement of contributions of the entire lithographic process and a better understanding of the resist-related processes and their impact on RLS performances. The development of computational tools is also of interest to confront observational results. Ultimately this approach will allow a more in-depth understanding of exposure contributions as we approach the sub-10 nm feature resolution limit for high-NA EUVL. Decoupling the two components of the lithographic process will allow for better understanding of the resist performance and tool performance and thereby contribute to further optimization and improvements.

REFERENCES

- [1] Schoot, J. V., Setten, E. van, Troost, K., Lok, S., Stoeldraijer, J., Peeters, R., Benschop, J., Zimmerman, J., Graepner, P., Wischmeier, L., Kuerz, P. and Kaiser, W., "High-NA EUV lithography exposure tool: program progress," Extreme Ultraviolet (EUV) Lithography XI **11323**, 1132307, International Society for Optics and Photonics (2020).
- [2] Higgins, C. D., Szmanda, C. R., Antohe, A., Denbeaux, G., Georger, J. and Brainard, R. L., "Resolution, Line-Edge Roughness, Sensitivity Tradeoff, and Quantum Yield of High Photo Acid Generator Resists for Extreme Ultraviolet Lithography," Jpn. J. Appl. Phys. **50**(3R), 036504 (2011).
- [3] Wallow, T., Higgins, C., Brainard, R., Petrillo, K., Montgomery, W., Koay, C.-S., Denbeaux, G., Wood, O. and Wei, Y., "Evaluation of EUV resist materials for use at the 32 nm half-pitch node," Emerging Lithographic Technologies XII **6921**, 69211F, International Society for Optics and Photonics (2008).

- [4] Santaclara, J. G., Geh, B., Yen, A., Brunner, T. A., Simone, D. D., Severi, J. and Rispens, G., “One metric to rule them all: new k4 definition for photoresist characterization,” *Extreme Ultraviolet (EUV) Lithography XI* **11323**, 113231A, International Society for Optics and Photonics (2020).
- [5] Wang, X., Tseng, L.-T., Allenet, T., Mochi, I., Vockenhuber, M., Yeh, C.-K., Lent-Protasova, L. van, Santaclara, J. G., Custers, R. and Ekinci, Y., “Progress in EUV resists status towards high-NA EUV lithography,” *Extreme Ultraviolet (EUV) Lithography XI* **11323**, 113230C, International Society for Optics and Photonics (2020).
- [6] Langner, A., Solak, H. H., Gronheid, R., Setten, E. van, Auzelyte, V., Ekinci, Y., Schenau, K. van I. and Feenstra, K., “Measuring resist-induced contrast loss using EUV interference lithography,” *Extreme Ultraviolet (EUV) Lithography* **7636**, 76362X, International Society for Optics and Photonics (2010).
- [7] Mojarad, N., Hojeij, M., Wang, L., Gobrecht, J. and Ekinci, Y., “Single-digit-resolution nanopatterning with extreme ultraviolet light for the 2.5 nm technology node and beyond,” *Nanoscale* **7**(9), 4031–4037 (2015).
- [8] Hoffnagle, J. A., Hinsberg, W. D., Houle, F. A. and Sanchez, M. I., “Characterization of photoresist spatial resolution by interferometric lithography,” *Metrology, Inspection, and Process Control for Microlithography XVII* **5038**, 464–472, International Society for Optics and Photonics (2003).
- [9] Sanchez, M. I., Hinsberg, W. D., Houle, F. A., Hoffnagle, J. A., Ito, H. and Nguyen, C. V., “Aerial image contrast using interferometric lithography: effect on line-edge roughness,” *Advances in Resist Technology and Processing XVI* **3678**, 160–171, International Society for Optics and Photonics (1999).
- [10] Mochi, I., Vockenhuber, M., Allenet, T. and Ekinci, Y., “Open-source software for SEM metrology,” *Photomask Technology 2020* **11518**, 115180G, International Society for Optics and Photonics (2020).